Low-frequency Raman spectra in $LiNbO_3$: Within and beyond the standard paradigm of ferroelectric dynamics

N. V. Surovtsev,[1] A. M. Pugachev,[1,2] V. K. Malinovsky,[1] A. P. Shebanin,[3] and S. Kojima[2]
[1]*Institute of Automation and Electrometry, Russian Academy of Sciences, Novosibirsk, 630090, Russia*
[2]*Institute of Material Science, University of Tsukuba, Tsukuba, Ibaraki 305-8573, Japan*
[3]*United Institute of Geology, Geophysics, and Mineralogy, Russian Academy of Sciences, Novosibirsk, 630090 Russia*
(Received 13 April 2005; revised manuscript received 21 June 2005; published 27 September 2005)

Low-frequency Raman spectra of stoichiometric $LiNbO_3$ crystals are investigated in the frequency range down to ~ 1 cm^{-1} and in the temperature range of 300–1423 K. The central peak (quasielastic light scattering) is found and described for all temperatures studied and in both scattering geometries explored, *zz*- and *xy*-configurations. The central peak features follow the standard paradigm, predicting the critical narrowing of the width, only at $T \gtrsim 1300$ K in the *zz*-configuration. At lower temperatures the inverse relaxation time increases with the temperature increase, in contradiction to the standard theoretical predictions. This experimental result was interpreted as the importance of local fluctuations of the order parameter. The ferroelectric dynamics of $LiNbO_3$ is described by the soft mode coupled to a relaxation, sharing both displacement and order-disorder features.

DOI: 10.1103/PhysRevB.72.104303 PACS number(s): 63.70.+h, 77.80.Bh, 77.84.Dy, 78.30.−j

I. INTRODUCTION

Lattice dynamics in ferroelectrics have some interesting features near the phase transition. These features have been the subject of intensive theoretical and experimental studies for a long time. Raman scattering is one of the most widely used experimental techniques of studing dynamics of ferroelectrics. There are two experimental features in Raman spectra which appear near the ferroelectric phase transition. First is the slowing down of the soft ferroelectrical mode. For crystals whose phase transition is governed by the evolution of the soft mode (displacement type of ferroelectrics), the temperature dependence of the soft mode frequency ω_T

$$\omega_T^2(T) \propto \varepsilon_z^{-1}(T) \tag{1}$$

is expected.[1] Equation (1) reflects Lyddane-Sachs-Teller relations with disregarding temperature dependencies of the nonsoft mode frequencies and of the high-frequency dielectric constant. In Eq. (1), ε_z is the low-frequency dielectric constant along the ferroelectric axis. The phenomenological theories, assuming the linear temperature dependence of the quadratic term of thermodynamical potential near the phase transition,[2,3] predict the Curie-Weiss law for ε_z and

$$\omega_T^2(T) \propto T_c - T, \tag{2}$$

where T_c is the phase transition temperature.

The dependence of Eq. (2) is often smeared by the appearance of an intensive central peak, which is the second typical feature of inelastic light scattering spectra near the phase transition.[4] This peak reflects some internal relaxational mode. The peak can appear in Raman scattering spectra via direct inelastic scattering of photons on a relaxational mode (direct mechanism) or as a low-frequency part of a damped harmonic oscillator coupled to a relaxational mode (indirect mechanism). If the relaxation mode is related to ferroelectric polarization, then critical slowing down is expected as the temperature approaches the phase transition. For crystals whose phase transition is governed by ordering of local dipoles (order-disorder type of ferroelectrics), the temperature dependence of the relaxational time τ of the mode associated with this ordering motion is predicted in the form[2,3]

$$\tau^{-1}(T) = \tau_0^{-1}[(T_c - T)/T_c]. \tag{3}$$

Phenomenological derivation of Eq. (3) implies the linear temperature dependence near the phase transition for the quadratic term of the thermodynamical potential [as for Eq. (2)]. The second assumption here is that the relaxational mode seen in Raman scattering is the same as the mode governing ferroelectric polarization. In some sense, the relaxational mode is the macroscopical one in this case. Also, in derivation of Eq. (3) by a possible energy barrier between the fluctuating state and the equilibrium one, is neglected.

In most studies of Raman spectra of ferroelectrics, the adherence to Eq. (2) or Eq. (3) is verified. Within the standard paradigm of ferroelectric dynamics, this procedure allows researchers to suggest the type of ferroelectrics (displacement or order-disorder character).

However, Eqs. (2) and (3) are derived only for a temperature range close to the phase transition. The validity limit for these equations is an interesting and important question. For a particular substance, it can be solved experimentally by studying the deviation of the Raman spectra from the predictions of Eqs. (2) and (3). Information about ferroelectric dynamics beyond the validity of Eqs. (2) and (3) is very important for the development of the ferroelectric dynamics theory. For example, at temperatures not close to the phase transition, ferroelectric fluctuations manifested in Raman spectra would be ruled mainly by local short-lived fluctuations that would have features different from those of macroscopic polarization relaxation. In particular, the energy barrier between the excited state of a crystalline cell and the equilibrium one[2] would be important.

Lithium niobate, $LiNbO_3$, is a very convenient material to study ferroelectric dynamics far from the phase transition.

This crystal has a single high-temperature phase transition occurring around 1470 K. The study of Raman spectra of $LiNbO_3$ has almost a 40 year history.[5,6] However, in spite of numerous works in which inelastic light scattering in lithium niobate was studied, the investigations of Raman spectra in the temperature range near the phase transition are relatively scarce.[6–10] To our knowledge only in three works[6,8,10] Raman spectra of $LiNbO_3$ near the phase transition, up to 1100–1200 K, were analyzed from the view point of the soft mode or relaxational dynamics [Eqs. (2) and (3)]. In the first work,[6] the ferroelectric transition was associated with zeroing of soft phonon modes, and it was shown that the "center-of-gravity" frequency of the *zz*-spectrum follows Eq. (2) with $T_c = 1480$ K. The use of the center-of-gravity frequency in this work instead of the soft mode frequency is caused by smearing of the soft mode peak in the low-frequency spectrum by the intensive central peak. In the work,[8] this difficulty was overcome by the analysis of spectral data within the model of a damped harmonic oscillator coupled with an interaction strength δ^2 to the relaxational mode. Hence, the response function has the form

$$\chi^{-1}(\omega,T) = \omega_0^2(T) - \omega^2 - i\omega\gamma_0(T) - \frac{\delta^2(T)}{1 - i\omega/\gamma_R(T)}. \quad (4)$$

The Stokes side of the Raman spectra is proportional to $(n+1)\mathrm{Im}[\chi(\omega,T)]$. In the work,[8] the form (4) was applied to a higher-frequency A_1 TO mode ($\sim$276 cm^{-1} at room temperature), assuming that this mode moves through the lower-frequency A_1 TO mode ($\sim$252 cm^{-1} at room temperature) near 600 K. The authors of Ref. 8 had found that the inverse relaxational time $\gamma_R(T)$ for a stoichiometric sample exhibits the critical slowing down of Eq. (3), while $\gamma_R(T)$ for a congruent sample is independent of temperature. δ^2 was found to follow $(T_c - T)^{-1.4}$ behavior in agreement with the prediction of Ref. 11. No behaviors like Eq. (2) were found in Ref. 8.

The results of Ref. 8 were questioned in a relatively recent study.[10] The authors of this work used the direct mechanism for the central peak in analyzing the experimental spectra, since they believed that "there is no argument to invoking a coupling between the relaxational mode and the lowest frequency phonon." The suggestion of the additional low-frequency contribution (in the range 40–100 cm^{-1}) was the novelty of Ref. 10 which allowed the authors to improve the quality of the spectra fitting. A significant softening of the lowest A_1 TO mode was found in this work, while the description of the $\omega_T(T)$ behavior via Eq. (2) provides T_c much higher than the real Curie temperature of $LiNbO_3$. In the work,[10] the relaxational mode was described to exhibit the critical slowing down of Eq. (3) with the critical temperature of 1310 K.

Thus, in spite of the long history of Raman scattering investigation in $LiNbO_3$, the behavior near the phase transition is not clear. There are different descriptions and points of view about the low-frequency crystal dynamics. Moreover, the studies[6,8,10] most significant in this respect are restricted by the temperature range of $\sim$1100 K, and the range of 1200–1450 K is not covered. Also, the low-frequency limit of these studies is $\sim$10 cm^{-1}; it will be shown in our work that this limitation can cause significant misestimation of the central peak width. It is necessary to reinvestigate low-frequency inelastic light scattering in $LiNbO_3$, including higher temperatures and lower frequencies.

In our recent investigation[12] of the low-frequency Raman spectra in $LiNbO_3$, the existence of the central peak was also found at room temperature and lower. This peak has some different features in comparison with those observed for the central peak at higher temperatures (in the works,[8,10] the central peak parameters were determined starting from 500 K). In particular the central peak is present for all Raman scattering geometries, so it cannot be ascribed to direct scattering from pristine ferroelectric relaxation. Moreover, the low-temperature extrapolation of the relaxational time from the high-temperature data of Ref. 10 provides a much wider width of the central peak in comparison with experimental data.[12] There is a need to "overlap" the high-temperature and low-temperature scenarios of the central peak behavior.

Thus, it is necessary to experimentally investigate the central peak in the Raman spectra of $LiNbO_3$, to cover the temperature range from room temperature to $\sim$1400 K and include both scattering geometries where phonons of A_1 and E symmetries are allowed. The present work deals with this task.

II. EXPERIMENT

Nearly stoichiometric lithium niobate crystals were grown by the double crucible Czochralski method and purchased from Oxide Corporation. The nominal $[Li_2O]:[Nb_2O_5]$ ratio is 49.9:50.1. Single crystals of lithium niobate $LiNbO_3$, being parallelepiped samples of high quality cut along crystallographic axes, were used in our study. Light scattering spectra were measured by three spectral apparatures. In all cases, inelastic light scattering was excited by an argon ion laser with a wavelength of 514.5 nm and a power of 100 mW.

(i) The spectra in the range of 0.1–17 cm^{-1} were measured using a 3+3 pass tandem Fabry-Perot interferometer (Sandercock model) in a backscattering geometry. The samples were put into a tubular furnace with a temperature variation to 1423 K and stability of ±0.5 K. The scattering geometries used were $x(zz)\bar{x}$ and $x(zy)\bar{x}$. Two free spectral ranges (FSR) were used. FSR$\approx$1.1 cm^{-1} was applied mainly to get information about Brillouin lines, and FSR$\approx$10 cm^{-1} was used to study the central peak.

(ii) U1000 a double Raman spectrometer and a hand-made oven with a temperature variation to 1150 K were used to study the Raman spectra in the scattering geometries $x(zz)y$ and $z(xy)x$. At the low frequency range, the spectral slit of $\sim$1 cm^{-1} were used. The elastic line contribution due to the real instrumental response was typically negligible in comparison with the inelastic signal at $\omega > 3$ cm^{-1} for the $x(zz)y$ geometry and at $\omega > 3.5$ cm^{-1} for $z(xy)x$.

(iii) DFS-24 a double Raman spectrometer was equipped by a hand-made oven, which allowed us to reach a temperature of $\sim$1423 K. This spectrometer was used to extend the temperature range in comparison with experiment (ii). Spectral slits of $\sim$1 cm^{-1} were used. At high temperatures

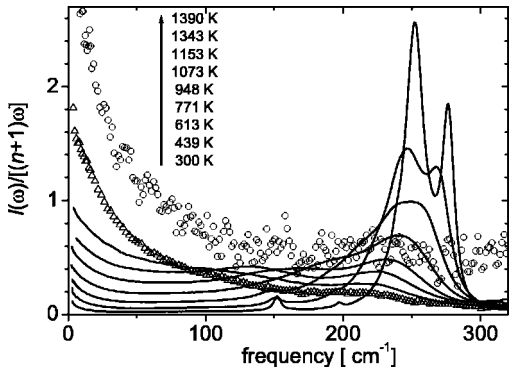

FIG. 1. Representative Raman spectra of $LiNbO_3$ at different temperatures in the $x(zz)y$ configuration. The spectra are shown at $T=300$, 439, 613, 771, 948, 1073, 1153, 1343, and 1390 K from bottom to top in the low-frequency part of the spectra.

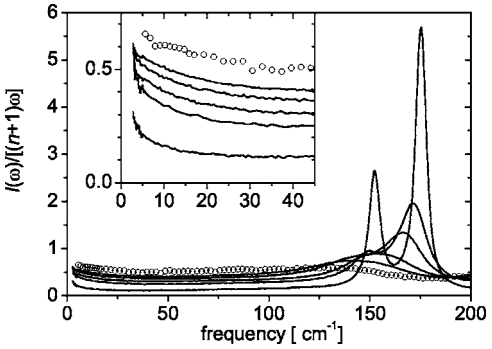

FIG. 2. The Raman spectra of $LiNbO_3$ at different temperatures in the $z(xy)x$ configuration. The spectra are shown at $T=300$, 548, 667, 873, 1003, and 1220 K from bottom to top in the low-frequency part of the spectra. The inset shows the central peak in details.

(>700 K), the elastic line contribution was negligible at $\omega > 5-6$ cm^{-1}. The contribution of heat radiation at high temperatures was determined by measuring in the absence of the exciting laser beam and was subtracted from raw data. The thermal background was not a sever problem by two reasons. First, in lithium niobate the Raman scattering intensity is quite strong. Secondly, we used the experimental geometries where hot parts of the ovens are not seen in the solid angle, within which the scattered light is collected, so the only radiant emittance of lithium niobate defines the heat radiation intensity, which is quite weak. This experimental geometry is possible for ovens with the horizontal windows, which were used in our experiments.

It was checked that the Raman spectra measured in experiments (ii) and (iii) were in good agreement, when the same temperatures were applied.

III. RESULTS AND ANALYSIS

The general view of Raman spectra is the same as in the previous works.[6–10] Figure 1 shows the typical Raman spectra of lithium niobate in the $x(zz)y$ configuration at different temperatures [note, that the small peaks at ~150 and 200 cm^{-1} do not belong to A_1 (TO) modes and appear due to polarization selection breakdown]. The spectral density presentation $I_n(\omega)=I(\omega)/[(n+1)\omega]$ is used in the figure to exclude the trivial temperature dependence for the vibrational spectra {here, $n=[\exp(h\omega/kT)-1]^{-1}$ is the Bose factor}. The spectral intensity for the spectra at different temperatures was normalized by the integral over the 0–400 cm^{-1} range without the frequency-independent background whose contribution is seen for the spectra at temperatures higher than 1350 K (we surmise that this contribution has the photoluminescence origin). The main temperature evolution of the spectra in Fig. 1 is related to the strong softening and broadening of two phonon modes as the temperature increases. The intensive central peak dominates in the Raman spectra at high temperatures. Moreover, the presence of the central peak is well seen even at low temperatures down to room temperature. The central peak at low temperatures was not reported in the previous works[6,8,10] probably because of limitations of the spectral range and the experimental sensitivity.

The second important experimental feature of the central peak is its dependence on the polarization configuration. We found that the central peak is also present in the $z(xy)x$ configuration where phonons of E-symmetry are allowed for Raman scattering. It was reported in Ref. 10 that the central peak is absent for this geometry of the Raman scattering experiment. However, the Raman signal in the $z(xy)x$ configuration is more than one order lower in comparison with the $x(zz)y$ configuration, which hinders the central peak registration for the $z(xy)x$ geometry. Nevertheless, as is illustrated in the inset of Fig. 2, the central peak is also present in the $z(xy)x$ Raman spectra. The distinction from the central peak in the $x(zz)y$ configuration is that its contribution is lower.

The existence of the central peak even at relatively low temperatures was confirmed by the measurements with a Fabry-Perot interferometer. These spectra are in agreement with Raman spectrometer data as is illustrated in Fig. 3. To emphasize the low-frequency part of the spectra, logarithmic

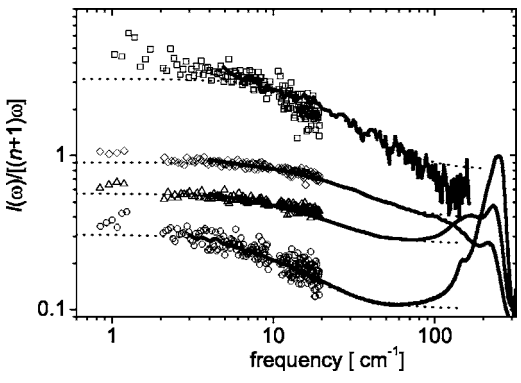

FIG. 3. Low-frequency part of Raman spectra at several typical temperatures. The lines correspond to the spectra recorded by the grating spectrometer [$x(zz)y$ configuration], and the symbols correspond to the measurements by the Fabry-Perot interferometer [$x(zz)\bar{x}$ configuration]. The spectra are shown at $T=613$, 963, 1153, and 1390 K from bottom to top in the low-frequency part of the spectra. The dotted lines are fitting curves for the central peak by Eq. (5).

scales are used in this figure. The gaps in the spectra near ~ 2 cm^{-1} correspond to the cut spectral range where intensive Brillouin lines dominate.

It is well seen from Fig. 3 that the behavior of the central peak width contradicts the previous reports and the predictions of the standard theories. The width increases as the temperature increases at least up to $T \sim 1200$ K. To obtain a quantitative description of the central peak behavior, a fitting procedure is needed. As was discussed in the Introduction, different approaches were applied for the central peak fitting in the case of Raman spectra from $LiNbO_3$, and sometimes the different behavior of the found parameters is attributed to the choice of the fitting procedure. We will discuss the outcomes of two different approaches to fitting, corresponding to direct and indirect mechanisms, and will show that the main experimental features are the same.

A. Direct mechanism analysis

We are starting from the description of the central peak by the direct mechanism. In this case, the spectrum is considered as a sum of damped harmonic oscillators and the relaxation mode. In this case, 11 parameters are needed to fit the Raman spectra of $LiNbO_3$ in the frequency range of $0-400$ cm^{-1}: 3 parameters (position, amplitude, and width) for each phonon mode (252, 276, 300 cm^{-1}), and 2 parameters for the relaxation mode. It was found in the work[10] that the use of only phonon modes and Debye relaxation is not sufficient for the perfect fitting of experimental spectra. The authors of this work introduced an additional phononlike mode attributed to a second-order process. In this case, the number of parameters becomes too large: 14. The problem of the large number of fitting parameters is especially topical for fitting high-temperature data, where the phonon modes become broad and hardly defined. If one is only interested in central peak parameters, an oversimplified but well working approach can be applied, fitting solely the central peak by a Debye relaxation. The most important advantage of this procedure is the minimum of number of fitting parameters needed. Also, this procedure facilitates the comparison between the Raman and Fabry-Perot experimental results. Figure 4 shows the results of fitting the central peak by the expression

$$\chi_R''(\omega)/\omega = \frac{2A}{\pi\gamma_R}\frac{1}{1+(\omega/\gamma_R)^2} + C, \qquad (5)$$

where A is the integral contribution of the relaxation mode in the Stokes part of the spectrum (in Figs. 4 and 5, the integral over spectral intensity is taken as the unit), γ_R is the half-width half-maximum corresponding to the inverse relaxation time, and the constant C is the simplest approximation for the contributions of the tails from the phonon modes and/or of the second order processes. Examples of fitting are shown in Fig. 3, where the fitting procedure was applied for Raman data in the range of $6-60$ cm^{-1} (fitting curves are shown in an extended range for illustration).

It should be noted that the values of the parameters depend on the spectral range selected for fitting. The disagreement of the parameters for different fitting ranges is not crucial and originates mainly from the assumption that the contribution C is independent of frequency. In Fig. 4(b), the fitting parameters both for the Fabry-Perot interferometer experiment (fitting range $1-19$ cm^{-1}) and for the Raman experiment (typical fitting range $6-60$ cm^{-1}) are shown. It is well seen that, while the absolute values are somehow different, they follow the same behavior, differing only by a temperature-independent shift. This result confirms that the approximation of Eq. (5) offers a fairly accurate description of the main features of the central peak.

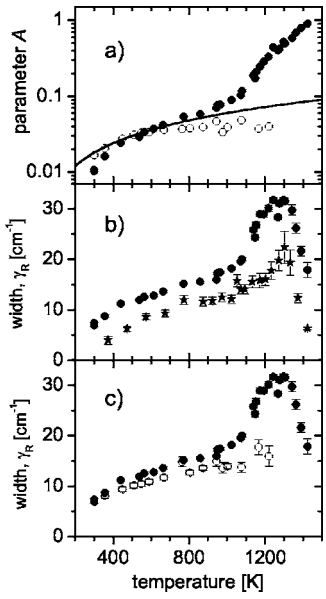

FIG. 4. Temperature dependences of the parameters for the central peak described by Eq. (5). (a) The integral intensity of the central peak in the $x(zz)y$ and $z(xy)x$ configurations (solid and open circles, respectively). The line is the curve $\propto T$. (b) The relaxation width in (zz)-experiments. The circles correspond to Raman experiment and the stars to the Fabry-Perot interferometer data. (c) The width of the central peak in the $x(zz)y$ and $z(xy)x$ configurations (solid and open circles, respectively).

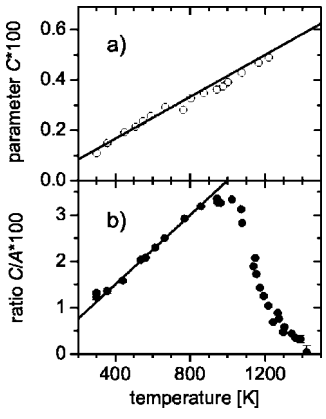

FIG. 5. Temperature dependences of the parameters for the central peak described by Eq. (5). (a) Parameter C for the central peak in the $z(xy)x$ configuration. The line is the curve $\propto T$. (b) Ratio of C and A parameters versus temperature for the central peak in the $x(zz)y$ configuration. The line is the curve $\propto T$.

The integral intensity of the central peak (parameter A) sharply increases with the temperature in the configuration, where "ferroelectric" phonon modes of A-symmetry are allowed for Raman scattering. To visualize the whole temperature behavior of the parameter A, the logarithmic scale for the intensity is used in Fig. 4(a). It is seen that a rather moderate temperature increase in relaxation intensity becomes much sharper in the temperature range above ~1000 K. The behavior of relaxation intensity in the experimental configuration, where phonon modes of E-symmetry are allowed, is similar in the range up to ~1000 K [Fig. 4(a)]. The minor difference is that the temperature dependence of relaxation intensity in "ferroelectric" spectra is slightly super-linear, while in "nonferroelectric" spectra it is slightly sublinear. The main difference is the behavior in the range above ~1000 K, where there is no sharp increase of relaxation intensity in "nonferroelectric" spectra.

One of the striking results is the temperature dependence of the central peak width, which has a nonmonotonic behavior. It increases moderately with temperature up to ~1000 K and then starts to rise more sharply up to 1200–1300 K. And only above the temperature of ~1300 K does the width decrease, following the standard model predictions. The width of the central peak in the $z(xy)x$ geometry shows only a moderate increase with temperature and no sharp increase above ~1000 K.

It is interesting to investigate the temperature dependence of the constant C from Eq. (5). If the assumption of Ref. 10 is valid, and, therefore, C reflects mainly the second-order contribution, one should expect a quasilinear temperature dependence for $C(T)$. This prediction is fair if the anharmonicity for the effective potential of vibrations is not changed significantly with temperature. As is shown in Fig. 5(a), indeed, $C(T)$ is linear for the $z(xy)x$ configuration of the Raman experiment, corroborating the assumption of Ref. 10. However, in the case of the $x(zz)y$ experiment, $C(T)$ increases much faster with temperature. A reasonable explanation would be that the factor of anharmonicity increases with temperature. It is well expected for "ferroelectric" modes since the anharmonicity is the driving factor of the ferroelectric transition. The temperature increase in relaxation intensity in some cases can be attributed to the increase in anharmonicity. By analogy with Fig. 5(a) it could be expected for the case of the $x(zz)y$ experiment that the ratio C/A is adequately described by a linear temperature dependence. As is seen from Fig. 5(b), indeed, this ratio follows the linear temperature dependence for the $x(zz)y$ configuration from room temperature to ~1000 K. Above this temperature, this ratio rapidly decreases, reflecting the dominating contribution of the central peak to the Raman spectra.

B. Damped oscillator analysis

The second analysis of the experimental Raman spectra of the $LiNbO_3$ crystal presented is the model of a damped harmonic oscillator coupled to a relaxational mode with the response function in the form of Eq. (4).[8] We found that the quality of spectrum fitting is the same for the direct and indirect mechanisms of the relaxation mode manifestation in inelastic light scattering spectra. So, it is impossible to choose the correct mechanism only from the quality of fitting for the experimental spectra. The second note is that the second-order contribution in the presented analysis is taken into account in the simplest frequency-independent approximation. This allows us to minimize the number of fitting parameters. As can be seen from the results of the previous subsection, this approximation is rather sufficient. Following Ref. 8, we used the approximation that only one mode has the coupling with the relaxational mode, which is lowest at high temperatures, and other modes have not. In contrast to Ref. 8, but in agreement with Ref. 10, the assumption that there is no crossing of two lowest modes of A-symmetry in $LiNbO_3$ was accepted in our analysis. The validity of this assumption will be evidenced by the results of the analysis.

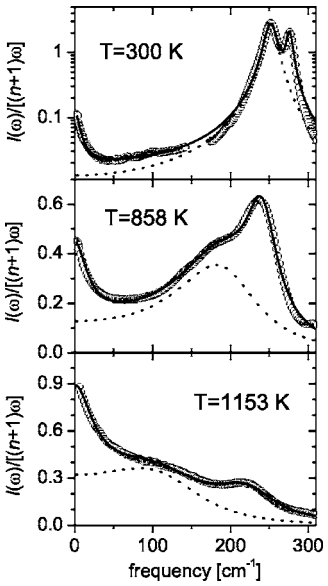

FIG. 6. Three examples of the experimental spectrum (circles) fitted by the damped oscillator model. The solid lines are the fits and dotted lines are the soft-mode response if $\delta^2=0$.

Three examples of fitting are shown in Fig. 6. To demonstrate the description of the central peak at room temperature, the logarithmic scale is used for the intensity in the top part of Fig. 6 [small peak at 150 cm^{-1} do not belong to A_1 (TO) modes and was cut from the experimental spectrum]. There is good agreement between the fitting curves and the experimental ones in Fig. 6. For illustration, the response of the soft mode in the absence of coupling with the relaxational mode ($\delta=0$) is also shown in Fig. 6. It is obvious that all fitting parameters in Eq. (4) are unambiguously defined from the experimental spectra at low temperatures owing to a significant spectral separation between the central peak and phonon modes. In the temperature range above ~1100 K, the soft phonon mode is not well separated from the central peak (Fig. 6, bottom), and the fitting parameters are interrelated. Some additional assumptions or restrictions are needed to correctly fit the spectra at $T>1100$ K. These assumptions can be found from the results of the analysis at $T<1100$ K.

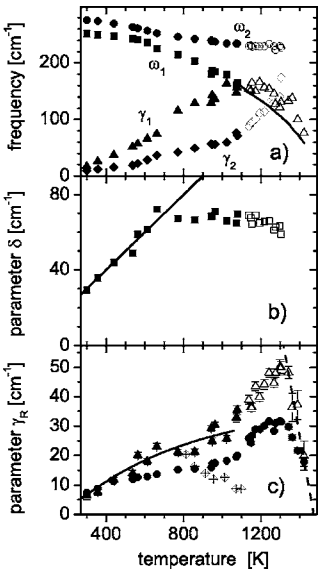

FIG. 7. Temperature dependence of the fitting parameters. The open symbols correspond to the fits where the parameter ω_1 was fixed, as is shown by the solid line in (a). (a) The frequency (circles and squares) and width γ (triangles and diamonds) for the two lowest A_1(TO) phonons. (b) Parameter δ. The solid line is the curve $\propto T$. (c) Inverse relaxation time γ_R. The triangles are the fits by the damped oscillator model and the circles by the "direct mechanism" analysis. The solid line is the fit by Eq. (6). The crossed diamonds are the data from Ref. 10. The dashed line is $\propto(1473-T)$.

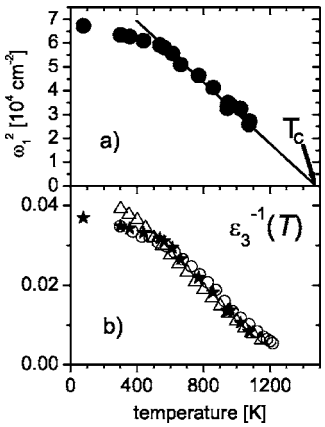

FIG. 8. (a) Temperature dependence of the soft-phonon frequency squared (circles). The line is $\propto(1473-T)$. (b) Temperature dependence of ε_3^{-1}, data from Ref. 14 (circles) and Ref. 15 (triangles). The stars are the parameter $\propto\omega_1^2-\gamma_1^2$ for the soft mode.

1. The temperature range of 300–1100 K

The temperature dependences of fitting parameters are shown by solid symbols in Fig. 7. The behavior of the phonon frequencies ω_1,ω_2 and width γ_1,γ_2 for two lowest A_1(TO) modes are in very good agreement with the data presented in Ref. 10. This agreement is important since different mechanisms (direct and indirect) and different ways of accounting for the second-order contribution were applied in Ref. 10 and in the present work. The agreement confirms the high level of validity of the present analysis. The agreement with data of Ref. 8 is worse in the range 700–1100 K because of ignoring the second-order contribution in Ref. 8, which leads to the overestimated phonon width in this work.

The parameter $\delta(T)$ governing the relative contribution of the relaxation mode into the spectra shows approximately a linear increase with temperature up to ~700 K [Fig. 7(b)]. At higher temperatures $\delta(T)$ is temperature-independent. This behavior of $\delta(T)$ is in contrast to that reported in Ref. 8. We checked that the spectra digitized from Ref. 8 at several temperatures are in rather good agreement with our corresponding spectra. So, the main difference in the reported values of $\delta(T)$ is related to ignoring the second-order contribution and, we guess, to an inaccurate way of the parameter choice in Ref. 8. A scarce number of temperature values presented in Ref. 8 makes a more detailed comparison difficult.

The temperature dependence of the inverse relaxational time γ_R is shown in Fig. 7(c). These data are compared with the direct mechanism analysis. Good qualitative agreement is seen between the data, while there is a difference at the quantative level. The difference can be attributed to different fitting ranges as was discussed in the previous subsection. $\gamma_R(T)$ demonstrates a moderate temperature increase, which becomes sharper above ~1000 K.

The found behavior $\gamma_R(T)$ differs from that reported in Ref. 10. The values of $\gamma_R(T)$ presented in Ref. 10 "from the fits with a large confidence" are shown in Fig. 7(c) for comparison. While the temperature range of the data from Ref. 10 is relatively short, 800–1100 K, it is well seen that they demonstrate a contrasty different temperature dependence with respect to the present work. The difference appeals to a comment. Partially, the difference found would be related to the specific way of taking into account the second-order contribution used in Ref. 10. It seems that more basic fits would show values of $\gamma_R(T)$ much closer to our data. We digitized the central peak curves plotted in Fig. 4 of Ref. 10, where they are presented for temperatures from 579 to 915 K. These spectra were fitted by Eq. (5), except for a few points near the elastic lines, where the dominating contribution of the elastic line is evident in Fig. 4 of Ref. 10. $\gamma_R(T)$ found in this fit is in excellent agreement with the data of the present work: γ_R monotonically increases from 13.5 cm^{-1} at $T=579$ K to $\gamma_R=16.8$ cm^{-1} at $T=915$ K. The second reason for the weakness for data in Ref. 10 is the contribution of the elastic line at the nearest frequencies and a rather short spectral range—the inverse relaxation time reported in Ref. 10 for T near 1100 K is smaller than the lowest limit of the spectral range studied.

The soft-mode frequency squared is shown in Fig. 8(a). Strong softening of ω_1^2 is seen from this picture. In the case of ferroelectrics of the displacement type, it should follow Eq. (2). In Ref. 10 the whole temperature range (300–1100 K) was applied for the description of ω_1^2 by Eq. (2) and a too high value $T_c\sim1700$ K was found from the fit. However, as is well seen from Fig. 8(a), it seems to be a change in the temperature dependence near ~550 K, and Eq. (2) should be applied only for the higher temperature range. Indeed, in the range of 550–1100 K $\omega_1^2(T)$ is in good agreement with the behavior of Eq. (2) with $T_c=1473$ K, as is

shown in Fig. 8(a) by the straight line (we used the value of 1473 K as the temperature of the ferroelectric transition for the stoichiometric $LiNbO_3$, while other values are also reported in the literature varying typically by ~10–20 K). Thus, the behavior of the soft mode in the range up to ~1100 K follows well the displacement-type scenario for the phase transition. This result encouraged us to compare the dielectric data with the renormalized frequency $\omega_0^2=\omega_1^2-\gamma_1^2$, which is expected to govern the low-frequency susceptibility.[13] In Fig. 8(b), the inverse dielectric permittivity ε_z^{-1} measured at low frequency in the work[14] (100 kHz) and the work[15] (10 MHz) is presented. This figure displays good agreement for the temperature behavior of $\varepsilon_z^{-1}(T)$ and $\omega_0^2(T)$.

2. The temperature range of **1100–1423 K**

As is discussed above, in this temperature range there is the problem of a too large number of fitting parameters in the case of a weakly structured spectrum. There is a need of ad hoc assumptions reducing the number. The behavior of $\omega_1^2(T)$ following Eq. (2) in Fig. 8(a) allows us to extrapolate this behavior to higher temperatures. This assumption was used for the temperature range above 1100 K, and the parameters obtained from this fit are shown in Fig. 7 by open symbols. It is seen that the behavior of the parameters at $T>1100$ K reasonably continues the lower temperature dependence. Above ~1300 K, the second phonon mode becomes strongly damped, and its spectral contour is ill-defined, that results in the necessity of reducing again the number of fitting parameters. For this temperature range, we used the simplest approximation of a frequency-independent contribution from the second ferroelectric mode in the low-frequency part of the Raman spectrum, and the highest temperatures (1300–1423 K) were fitted with this assumption. Since the credibility value of this assumption can crucially influence the parameters like the relative integral contribution of different modes, such parameters are not presented and are not discussed in this temperature range.

Since applying assumptions could distort the extracting results, we checked: What we obtain, if we suppose a contrasty different case that at $T>1100$ K ω_1 is temperature independent and equal to $\omega_1(T=1100\ \mathrm{K})$. It was found that the qualitative behavior of the parameters in most cases is the same with a significant difference, certainly, at the quantitative level. It confirms the high level of confidence for the results presented below. One exception is the behavior of γ_1, which continues the sharp rise for the case of the last assumption. For the main assumption, the temperature dependence of the parameter γ_1 follows the assumed behavior of ω_1, keeping the ratio approximately $\gamma_1/\omega_1\sim 1$ [Fig. 7(a)].

The whole temperature dependence of the inverse relaxation time mimics the behavior of γ_R found in the direct mechanism analysis. In particular, it confirms the sharp decrease above ~1300 K. The decrease of γ_R in approaching the ferroelectric transition temperature is compatible with the critical slowing down of $\gamma_R(T)\propto(T_c-T)$ shown by the dashed line in Fig. 7(c) for $T_c=1473$ K. Thus, independently of the fitting scenario [Figs. 5(b) and 7(c)], the main features of $\gamma_R(T)$ are the same.

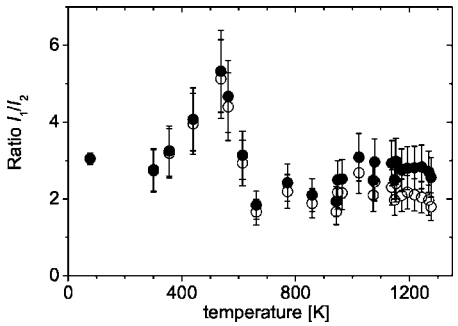

FIG. 9. Temperature dependence of the ratio between the integral intensities of two low-frequency phonon modes in the $x(zz)y$ configuration. The solid symbols correspond to the evaluation with the central peak is included into the lowest mode, and the open symbols correspond to the case with the central peak is not included into the lowest mode.

The behavior of $\delta(T)$ in the range of 1100–1300 K is the temperature-independent continuation of the lower temperature course. Let us consider the question different answers to which were suggested in Refs. 8,10—whether there exists the crossing of two phonon lines of A-symmetry near 550 K or an anticrossing occurs. We used the second case in our analysis and checked the ratio of integral intensities between the lowest (I_1) and second low one (I_2) phonon modes. The results of the temperature dependence of the ratio I_1/I_2 are shown in Fig. 9. If the assumption is true, this ratio should be the same below and above the apparent crossing (certainly, this ratio near $T\sim 550$ K is ill-defined, causing a singularity, as is seen in Fig. 9). If the assumption is invalid and the real crossing occurs, then one should expect the invertion of the ratio from 3 at low temperatures to 1/3 at high temperatures. It is seen from Fig. 9 shows that the second case is not realized, and the ratio with a satisfactory precision is the same at high and low temperatures (the ratio for 80 K was calculated using the data from Ref. 12). Figure 9 shows two versions of the calculation: with I_1 including the central peak (indirect mechanism) and excluding it (direct mechanism). The first case was calculated merely equating the found parameter δ to zero (examples are shown in Fig. 6). Therefore, our analysis supports the assumption of Ref. 10 about the anticrossing.

IV. DISCUSSION

In all variants of analysis applied to Raman spectra of $LiNbO_3$ crystal, the behavior of the inverse relaxational time compatible with Eq. (3) was found only in the temperature range above ~1300 K. It is interesting that 1300 K is exactly the temperature where the dielectric loss $\tan\delta$ in $LiNbO_3$ changes its behavior from increasing with temperature to sharply decreasing.[15] Also, 1300 K is a temperature where the spontaneous polarization P_s in $LiNbO_3$ changes its temperature behavior from an extremely weak temperature dependence at lower temperatures to a sharp decrease at $T>1300$ K.[16] Thus, the temperature of 1300 K is a particular temperature for $LiNbO_3$ crystal: only above this temperature the crystal is flexible with regard to spontaneous polarization

fluctuations. In this respect, it is not surprising that collective fluctuations implied in derivation of Eq. (3) are frozen below ~1300 K and provide a minor contribution to the relaxational response manifested in Raman spectra.

The standard textbook theories predict the critical slowing down near T_c, Eq. (3), the inverse relaxation time decreasing with the temperature increase at $T<T_c$. However, in contrast to the predictions, in our study the opposite behavior is found for $\gamma_R(T)$ in the wide temperature range 300–1300 K; the inverse relaxation time increases with the temperature increase. To our knowledge such behavior for the inverse relaxation time was not reported before. The confrontation of $\gamma_R(T)$ behavior with the theories appeals to a revision of the theoretical models of ferroelectric dynamics. The standard approach predicting Eq. (3) should be extended to describe the central peak in Raman spectra of $LiNbO_3$ at $T<1300$ K. One possible extension would be taking into account the possibility of local fluctuations, involving the motion of individual ions. These dynamics should be described by the local energy barrier between two states, and the inverse relaxational time will follow the activation law

$$\gamma_R = \gamma_R^{\infty} \exp(U/kT). \tag{6}$$

As is seen from Fig. 7(c), Eq. (6) with $\gamma_R^{\infty}=50$ cm^{-1} and the energy barrier $U/k=600$ K describes the experimental dependence $\gamma_R(T)$ reasonably well up to 1000–1100 K. At higher temperatures, more complex interplay of different modes must be taken into account. Note, that the combination of Eqs. (3) and (6) solely by an assumption of $\tau_0^{-1}=\gamma_R$, is not enough to describe the temperature dependence of the central peak width, which is presented in Fig. 7(c). It seems that the accounting of the local atomic displacements without long-range order becomes the important direction for ferroelectric field of reasearch (for example, Ref. 17).

In the approach where the relaxation mode is coupled with the soft phonon, parameter δ should reflect both the magnitude of the relaxational motion and the efficiency of relaxation-phonon coupling. In this respect, the linear increase at $T<600$ K could reflect the increase in efficiency of relaxation-phonon coupling, which becomes approximately temperature-independent at higher temperatures [Fig. 7(b)]. It is interesting that the temperature increase in $\delta(T)$ was predicted by the phonon anharmonicity model,[18] suggested for explanation of fast relaxation in glasses. In the framework of this model, the temperature increase is terminated at high temperatures due to high anharmonicity terms.[19]

Another striking founding of the present work is the renovation of the idea of the displacementlike behavior in $LiNbO_3$. Indeed, the temperature behavior of the soft phonon frequency is in excellent agreement with Eq. (2) in the range of 550–1100 K [Fig. 8(a)]. Moreover, there is good agreement between dielectric data and $\omega_T^2(T)$ in the whole range $T<1100$ K [Fig. 8(b)]. Thus, it can be maintained that the driving mechanism approaching the ferroelectric transition in $LiNbO_3$ is the displacement one, if the temperature range $T<1100$ K is considered. In this case, the apparent increase in spectral density seen in Fig. 4(a) under constant δ at $T>600$ K [Fig. 7(b)] is related to softening ω_1. Figure 10 illustrates a comparison of the apparent integral intensity of the central peak with the relaxational intensity I_r found by the fit within the damped oscillator analysis. In the latter case, I_r was calculated as the difference between the total integral of the fitting curve and that with $\delta=0$. Also, the relative contribution of the relaxation peak can be estimated by the parameter δ^2/ω^2 (for example, Ref. 20). Good qualitative agreement between different parameters is seen in Fig. 10, where the logarithmic scale is used for the ordinate. The solid curve in this figure corresponds to the estimation of δ^2/ω^2, using the extrapolation to higher temperatures of the temperature-independent value of δ^2 [Fig. 7(b)] and the behavior of $\omega_1^2 \propto (T-T_c)$ [Fig. 8(a)]. The solid curve in Fig. 10 reaches the value ~1 in the temperature range of ~1400 K and higher. It means that the relaxational motion dominates in the total spectral intensity at high temperatures. Thus, because of the coupling with relaxation the displacement scenario evolution of the soft mode turns to the pure relaxational mode at high temperatures. The order-disorder type of ferroelectric dynamics at $T>1300$ K is well seen for $\gamma_R(T)$.

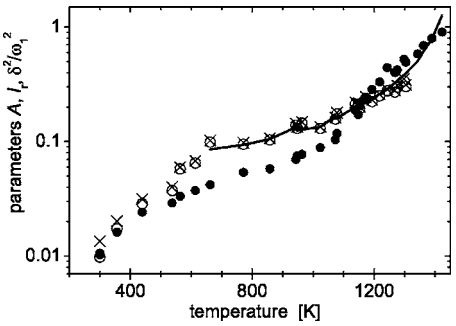

FIG. 10. Temperature dependence of the parameters A (solid circles), I_r (open circles), and δ^2/ω_1^2 (crosses). The solid line is the extrapolating curve $(66\ \text{cm}^{-1})^2/\omega_1^2$.

Figure 2 evidences that the E-phonon modes are also coupled to the relaxation mode, leading to the central peak appearance. Moreover, the relative contribution of the central peak to the Raman spectrum in the $z(xy)x$ configuration is comparable with that in the $x(zz)y$ configuration at $T<700$ K. The absence of softening of the E-phonon modes, however, leads to the absence of the increase in the central peak intensity above 600 K [Fig. 4(a)]. Thus, it is the difference in the temperature dependence of the phonon modes that is responsible for the different temperature behavior of the central peak for "ferroelectric" and "nonferroelectric" configurations of Raman experiment.

V. CONCLUSION

In the present work, a new study of the low-frequency Raman spectra in the ferroelectric $LiNbO_3$ crystal is presented with an emphasis on the central peak behavior. The central peak is studied in much extended spectral and temperature ranges than it was done before. Different approaches to the spectral analysis are presented and discussed. The new set of the central peak features is as follows:

(i) The inverse relaxation time increases with temperature up to ~1300 K, and only above this temperature the critical slowing down is observed.

(ii) In analysis by the damped oscillator coupled with the relaxational mode, the apparent temperature increase of the central peak intensity at $T>600$ K is caused by the soft mode softening, while the coupling parameter δ is temperature-independent.

(iii) The central peak is also seen in the $z(xy)x$ configuration, but its temperature behavior is different from that for the zz-configuration above 600–700 K and can be attributed to the absence of strong softening of E-phonons.

The most striking feature is the confrontation between the observed increases of the inverse relaxation time and the theoretical predictions for a wide temperature range 300–1300 K. Careful consideration, done in the work, evidences that this behavior is not an artefact of the experiment or analysis. Thus, the outcoming result call to revising the previous descriptions of the central peak features and to extending the standard paradigm of ferroelectric dynamics. In particular, taking into account local fluctuations of the order parameter would help to explain the low-temperature behavior of the central peak, which can be described by an activation motion with a single energy barrier at $T<1000$ K.

The ferroelectric dynamics of the $LiNbO_3$ crystal is well interpreted by a scenario where the soft mode is coupled to the relaxational mode. At low temperatures, the evolution is mainly governed by the phonon softening. At high temperatures, resonancelike reasons lead to pumping the spectral density into the relaxational mode, and the order-disorder-type of dynamics rules the critical narrowing of the central peak.

[1] C. Kittel, *Introduction to Solid State Physics* (Wiley, New York, 1986).
[2] M. E. Lines and A. M. Glass, *Principles and Application of Ferroelectrics and Related Materials* (Clarendon, Oxford, 1977).
[3] B. A. Strukov and A. P. Levanyuk, *Ferroelectric Phenomena in Crystals* (Springer, Berlin, 1998).
[4] *Light Scattering Near Phase Transition*, edited by H. Z. Cummins and A. P. Levanyuk (North-Holland, Amsterdam, 1983).
[5] A. S. Barker, Jr. and R. Loudon, Phys. Rev. **158**, 433 (1967).
[6] W. D. Johnston, Jr. and I. P. Kaminow, Phys. Rev. **168**, 1045 (1968).
[7] V. S. Gorelik, S. V. Ivanova, I. P. Kucheruk, B. A. Strukov, and A. A. Khalezov, Sov. Phys. Solid State **18**, 1340 (1976).
[8] Y. Okamoto, Ping-Chu Wang, and J. F. Scott, Phys. Rev. B **32**, 6787 (1985).
[9] Yu. K. Voron'ko, A. B. Kudryavtsev, V. V. Osiko, A. A. Sobol', and E. V. Sorokin, Sov. Phys. Solid State **29**, 771 (1987).
[10] A. Ridah, M. D. Fontana, and P. Bourson, Phys. Rev. B **56**, 5967 (1997).
[11] B. I. Halperin and C. M. Varma, Phys. Rev. B **14**, 4030 (1976).
[12] V. K. Malinovsky, A. M. Pugachev, A. P. Shebanin, and N. V. Surovtsev, Ferroelectrics **285**, 339 (2003).
[13] A. D. Bruce and R. A. Cowley, *Structural Phase Transitions* (Taylor and Francis, London, 1981).
[14] K. Nassau, H. J. Levinstein, and G. M. Loiacono, J. Phys. Chem. Solids **27**, 989 (1966).
[15] I. Tomeno and S. Matsumura, J. Phys. Soc. Jpn. **56**, 163 (1987).
[16] A. M. Glass (unpublished work), cited by J. G. Bergman, Chem. Phys. Lett. **38**, 230 (1976).
[17] E. A. Stern, Phys. Rev. Lett. **93**, 037601 (2004).
[18] V. N. Novikov, Phys. Rev. B **55**, R14685 (1997).
[19] V. N. Novikov, Phys. Rev. B **58**, 8367 (1998).
[20] V. N. Novikov, A. P. Sokolov, B. Strube, N. V. Surovtsev, E. Duval, and A. Mermet, J. Chem. Phys. **107**, 1057 (1997).